Magnetoelectronic excitations in single-walled carbon nanotubes

C. W. Chiu,[1] C. P. Chang,[2] F. L. Shyu,[3] R. B. Chen,[4] and M. F. Lin[1]
[1]*Department of Physics, National Cheng Kung University Tainan, Taiwan 701, Republic of China*
[2]*Center for General Education, Tainan Woman's College of Art & and Technology Tainan, Taiwan 71002, Republic of China*
[3]*Department of Physics, Chinese Military Academy Kaohsiung, Taiwan 830, Republic of China*
[4]*Center for General Education, National Kaohsiung Institute of Marine Technology Kaohsiung, Taiwan 830, Republic of China*
(Received 27 November 2002; published 28 April 2003)

The low-frequency single-particle and collective excitations of single-walled carbon nanotubes are studied in the presence of a magnetic field. They strongly depend on the magnitude and direction of the magnetic field, transferred momentum, temperature, nanotube geometry, and Zeeman splitting. A narrow-gap nonarmchair carbon nanotube exhibits two interband magnetoplasmons, while a metallic nonarmchair carbon nanotube exhibits one interband magnetoplasmon and one interband and intraband magnetoplasmon or two interband magnetoplasmons and one intraband magnetoplasmon. The differences among these plasmons are relatively obvious when the magnetic field is oriented closer to the nanotube axis. The transferred momentum determines the plasmon frequency and the existence of plasmons. The temperature can induce an intraband magnetoplasmon or change an interband magnetoplasmon into an intraband and interband magnetoplasmon.

DOI: 10.1103/PhysRevB.67.165421 PACS number(s): 73.20.Mf, 71.45.Gm

Quasi-one-dimensional (quasi-1D) carbon nanotubes have resulted in many interesting studies, mainly owing to the unique cylindrical structure.[1] The geometric structure[2–9] dominates over band structures. A (m, n) carbon nanotube is (I) a gapless metal for $m=n$, (II) a narrow-gap semiconductor for $m\neq n$ and $2m+n=3I$ (I an integer), and (III) a moderate-gap semiconductor for $2m+n\neq 3I$.[7–9] The magnetic field has a strong effect on electronic structures such as the variation of the energy gap, destruction of double degeneracy, and Zeeman splitting.[10–18] In this work, we mainly study the low-frequency electronic excitations of metallic or narrow-gap carbon nanotubes in the presence of a magnetic field. The dependence on the magnitude (B) and direction (α) of the magnetic field (**B**), temperature (T), transferred momentum (q), nanotube geometry (radius r and chiral angle θ), and Zeeman splitting is investigated.

The $2p_z$ and $(2s,2p_x,2p_y)$ orbitals in a sp^2 carbon nanotube, respectively, form the π and σ bands. The curvature effects, misorientation of $p\pi$ orbitals, and mixing of $p\pi$ and $sp^2\sigma$ orbitals significantly affect the low-energy π band except for armchair carbon nanotubes.[7–9] The elementary excitations in a cylindrical carbon nanotube have been studied within the random-phase approximation (RPA).[19–31] As a result of the cylindrical symmetry, there exist momentum- and angular-momentum-dependent π plasmons. Such plasmons have frequencies higher than 5 eV. They had been verified by the electron-energy-loss spectroscopy.[32–36] A metallic carbon nanotube is predicted to exhibit the low-frequency plasmon of zero angular momentum ($L=0$).[26] The effects due to curvature effects, magnetic field, and temperature are taken into account in this work.

The cylindrical carbon nanotubes resemble other quasi-1D electron systems, e.g., semiconductor quantum wires (QW's). The RPA is used to calculate the excitation spectra of QW's. They exhibit single-particle excitations and collective excitations (plasmons).[37–39] The frequencies and momentum dispersions are well consistent with resonant inelastic-light-scattering measurements.[40–42] These two kinds of excitations are expected to exist in carbon nanotubes. However, there are certain important differences between these two systems such as electronic excitations from different energy bands and curvature effects. Excitation modes of different L's are decoupled in a hollow carbon nanotube. This contrasts greatly with the complicated coupling among different electronic excitations in an ordinary QW.

We use the sp^3 tight-binding model to calculate the magnetoband structure of a single-walled carbon nanotube. A detailed description of the low-energy bands is found to be very important in understanding electronic excitations. The low-frequency electronic excitations are investigated by evaluating the longitudinal dielectric function (ϵ) within the RPA. The magnetic band-structure effects are strong and appreciably affect the characteristics of electronic excitations. Our study shows that the single-particle and collective excitations of $L=0$ are very sensitive to the changes in magnetic field, temperature, momentum, radius, and chiral angle.

The band structure of a (m, n) carbon nanotube is simply reviewed. It is obtained from the Slater-Koster tight-binding model with curvature effects (details in Ref. 9). Each carbon atom owns four valence electrons. The s orbital energy is $E_s=-7.3$ eV below the triply degenerate p orbitals taken as the zero of energy ($E_p=0$). The Slater-Koster hopping parameters for the nearest-neighboring pairs are $V_{ss\sigma}=-4.30$ eV, $V_{sp\sigma}=4.98$ eV, $V_{pp\sigma}=6.38$ eV, and $V_{pp\pi}=-2.66$ eV$(=-\gamma_0)$. A primitive unit cell has N_u carbon atoms, e.g., $N_u=4m$ for a $(m,0)$ zigzag nanotube. There exists the periodical boundary condition along the azimuthal direction ($\hat{\Phi}$). The 8×8 Hamiltonian matrix, which is related to the two nearest-neighbor carbon atoms, is sufficient in describing band structure in the absence of a magnetic field. Electronic states are characterized by the angular momentum $J(=1,2,...,N_u/2)$ and the longitudinal wave vector k_z $(-\pi\leqslant k_zR_z\leqslant\pi)$. R_z is the periodical distance along the nanotube axis ($\hat{z}$).

The magnetic field complicates the calculations of band structure when it is not parallel to the nanotube axis:[10–15,17–18] $\mathbf{B}=B\cos\alpha\hat{z}+B\sin\alpha\hat{\Phi}$, where α is the

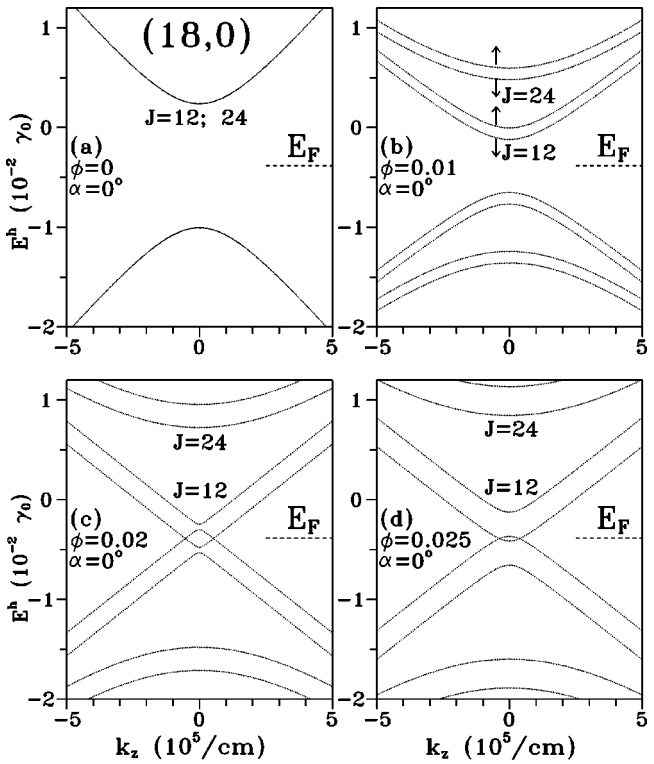

FIG. 1. Low-energy bands of $J=12$ and 24 for the (18, 0) zigzag nanotube at $\alpha=0°$ and (a) $\phi=0$, (b) $\phi=0.01$, (c) $\phi=0.02$, and (d) $\phi=0.025$. The unit of ϕ is ϕ_0, here and henceforth. The magnetic field corresponding to $0.01\phi_0$ is 26.5 T. The arrows in (b) represent the direction of spin.

angle between the magnetic field and nanotube axis. The parallel and perpendicular components, respectively, induce the shift $J\rightarrow J+\cos\alpha(\phi/\phi_0)$ and the coupling of different J's (details in Refs. 17 and 18): $\phi=\pi r^2 B\cos\alpha$ and $\phi_0=hc/e$. The vector potential is $\mathbf{A}=rB\cos\alpha/2\hat{\Phi}+rB\sin\alpha\sin(x/r)\hat{z}$ ($x=r\Phi$). The x or Φ dependence means that all carbon atoms in a primitive unit cell need to be taken into account in the Hamiltonian matrix elements. Moreover, the magnetic phase factor due to **A** would make the angular momenta mix with one another. The subindices of the Hamiltonian matrix depend on the angular momenta, the two nearest-neighbor sites A and B, and the four electron orbitals. The tight-binding Hamiltonian is characterized by a $4N_u\times 4N_u$ Hermitian matrix. Several previous studies[10–15] used the $N_u\times N_u$ Hamiltonian matrix within the $2p_z$ tight-binding model. They neglect the change of $V_{pp\pi}$ due to the misorientation of $2p_z$ orbitals and the hybridization of $p\pi$ and $sp^2\sigma$ orbitals. The curvature effects play an important role on the low-energy band structures and electronic excitations. The energy dispersion $E^{c,v}(J,k_z)$ and wave function $\Psi^{c,v}(J,k_z)$ are obtained by diagonalizing the Hamiltonian matrix. v (c) corresponds to the occupied valence band (the unoccupied conduction band). The Zeeman energy has to be added in the energy dispersion.[18] State energy is denoted as $E^h(J,k_z,\sigma)$.

The (18, 0) zigzag nanotube is chosen for a model study. The low-energy band structure is shown in Fig. 1 at $\alpha=0°$ and various ϕ's. There are doubly degenerate energy bands of $J=12$ and 24 at zero magnetic field [$\phi=0$ in Fig. 1(a)]. The occupied valence bands are approximately symmetric to the unoccupied conduction bands about the Fermi level [$E_F(\phi=0)=-0.004\gamma_0$]. Their energy dispersions are parabolic at small k_z and linear at others. Edge states are located at $k_z=0$, and the energy gap is $E_g=0.01\gamma_0$. Here E_g and parabolic energy bands completely come from the curvature effects.[9] When the magnetic field is parallel to the nanotube axis, the effects of ϕ on angular momenta J and $N_u/2-J$ are different. Hence the double degeneracy is destroyed at $\phi=0.01\phi_0$ [Fig. 2(b)]. The $J=12$ energy bands approach to the Fermi level, while the $J=24$ energy bands exhibit the opposite behavior. The energy gap is reduced by ϕ. The Zeeman effect results in the splitting of spin-up and spin-down states. The Fermi level $E_F(\phi)$ keeps at the center of the conduction and valence bands, and the $k_z=0$ edge states remain unchanged (even for $\alpha\neq 0°$). The spin-up valence band and spin-down conduction band of $J=12$ begin to touch at $\phi_1=0.0167\phi_0$ and overlap at $\phi=0.02\phi_0$ [Fig. 1(c)]. The overlap of energy bands is purely due to the Zeeman splitting. It is maximum at $\phi=0.0205\phi_0$. These two bands gradually depart from the Fermi level in the further increase of ϕ [$\phi=0.025\phi_0$ in Fig. 2(d)]. The overlap of energy bands vanishes at $\phi_2=0.026\phi_0$. The (18, 0) zigzag nanotube is metallic at $\phi_1\leqslant\phi\leqslant\phi_2$ and $\alpha=0°$.

The energy gaps and state degeneracy also depend on the direction of the magnetic field.[17,18] The shift of angular momentum, $J\rightarrow J+\cos\alpha(\phi/\phi_0)$, becomes small as α increases from 0°. The dependence of energy gap on magnetic flux is relatively weak at large α. For example, at $\phi=0.01\phi_0$, the (18, 0) zigzag nanotube has the smallest E_g at $\alpha=0°$ and the largest E_g at $\alpha=90°$. The smaller shift of J also leads to the gradual recovery of state degeneracy. The double degeneracy is recovered at $\alpha=90°$. On the other hand, the coupling of different J's becomes important in the increasing of α. Each energy band is composed of different J's. However, at small $\phi(<0.1\phi_0)$, the coupling effect is negligible for any α. That is to say, energy bands are well described by the discrete angular momenta.

For electrons on a cylindrical nanotube, the transferred momentum and angular momentum are conserved in the e-e Coulomb interaction.[19–26] Electronic excitations thus have the well-defined q and L. They are focused on the low-frequency modes of $L=0$. The magnetic longitudinal dielectric function within the RPA is given by

$$\begin{aligned}\epsilon(q,\omega;\phi,\alpha)&=1-4\pi e^2 I_0(qr)K_0(qr)\\&\times\sum_{J,\sigma,h,h'}\int\frac{dk_z}{(2\pi)^2}|\langle J,k_z+q,\sigma,h'|e^{iqz}|J,k_z,\sigma,h\rangle|^2\\&\times\frac{f(E^{h'}(J,k_z+q,\sigma;\phi,\alpha))-f(E^h(J,k_z,\sigma;\phi,\alpha))}{E^{h'}(J,k_z+q,\sigma;\phi,\alpha)-E^h(J,k_z,\sigma;\phi,\alpha)-\omega-i\Gamma}.\end{aligned}\tag{1}$$

$I_0(qr)$ [$K_0(qr)$] is the modified Bessel function of the first [second] kind of zero order. $\Gamma(=0.005\gamma_0)$

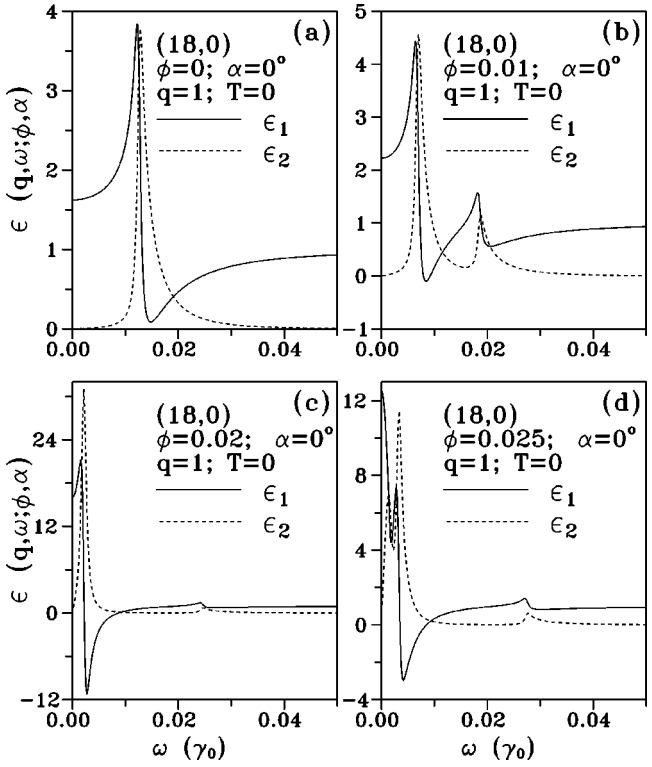

FIG. 2. Dielectric function of the (18, 0) zigzag nanotube at $q=1$, $T=0$, $\alpha=0°$ and (a) $\phi=0$, (b) $\phi=0.01$, (c) $\phi=0.02$, and (d) $\phi=0.025$. The real and imaginary parts are, respectively, shown by the solid and dashed curves. The unit of q is 10^5/cm, here and henceforth.

is the energy width due to various deexcitation mechanisms. The Fermi-Dirac function is $f(E^h(J,k_z,\sigma;\phi,\alpha))=1/\{\exp[E^h(J,k_z,\sigma;\phi,\alpha)-E_F(\phi,\alpha,T)/k_BT]+1\}$. Here E_F varies with magnetic field and temperature. The coupling of different J's is taken into account in the calculations of Eq. (1), although it is very weak. The unit of q is 10^5/cm in the following results.

The real $[\epsilon_1]$ and the imaginary $[\epsilon_2]$ parts of the dielectric function of the (18, 0) zigzag nanotube are shown in Fig. 2(a) at $\phi=0$, $\alpha=0°$, $T=0$, and $q=1$. Electrons are excited from the occupied valence bands to the unoccupied conduction bands of the same J's [Fig. 1(a)]. Only one interband excitation channel exists. The threshold single-particle excitations result from the $k_z=0$ edge state. They induce a prominent peak in ϵ_2 at the threshold excitation energy $\omega_{ex}=E^c(J,q)-E^v(J,0)$, owing to the 1D characteristic of the parabolic energy dispersions. The single-particle excitation energy is mainly determined by the detailed electronic structures. A simple relation between ω_{ex} and q is absent, since energy dispersions are not completely parabolic or linear. The corresponding ϵ_1 drastically changes from a large positive value to a small positive value (or a negative value at $\Gamma\rightarrow 0$). The small ϵ_1 and ϵ_2 can appear simultaneously, which, thus, leads to a prominent plasmon peak in the loss spectrum [Fig. 3(a)].

The destruction of state degeneracy and the overlap of energy bands due to a parallel magnetic field are directly reflected in the single-particle excitations. At $\phi=0.01\phi_0$, the splitting energy bands of $J=12$ and 24 [Fig. 1(b)], respectively, induce two different interband excitation channels at lower and higher excitation energies. As a result, there are two peak structures in ϵ_2 [Fig. 2(b)]. The spin-up and spin-down states in a semiconducting carbon nanotube have the identical interband excitations: i.e., they do not alter the number of excitation channels. However, for a metallic nanotube [Figs. 1(c) and 1(d)], the overlap of the spin-up $J=12$ valence band and the spin-down $J=12$ conduction band produces a new intraband excitation channel [Figs. 2(c) and 2(d)]. At $\phi=0.02\phi_0$ and $\phi=0.025\phi_0$, ϵ_2 exhibits a prominent peak at the lowest excitation energy. This peak is related to the $k_z=k_F$ state (the Fermi momentum state), but not the $k_z=0$ edge state. The origin of the strong single-particle excitations is different for intraband excitations and interband excitations. It is also noticed that at $\phi=0.02\phi_0$, the threshold excitation energy of the intraband excitations is almost the same with that of the interband excitations. The superposition of these two kinds of excitations causes a very sharp peak in ϵ_2 [Fig. 2(c)].

The loss function, which is defined as $\mathrm{Im}[-1/\epsilon]$, describes the collective excitation spectrum. Figure 3(a) presents the loss function of the (18, 0) zigzag nanotube at $q=1$, $T=0$, $\alpha=0°$, and various ϕ's. There is a pronounced peak in the absence of magnetic flux. It is associated with the small ϵ_1 and ϵ_2. This peak is identified as an interband plasmon. It corresponds to the collective excitations of the degenerate energy bands of $J=12$ and 24. One plasmon peak changes into two plasmon peaks as ϕ increases from zero, e.g., the loss spectra at $\phi=0.005\phi_0$ and $0.01\phi_0$. The $J=24$ and 12 energy bands, respectively, produce the first magnetoplasmon with higher frequency (ω_{p1}) and the second magnetoplasmon with lower frequency (ω_{p2}). Here ω_{p1} clearly increases as ϕ grows. The opposite is true for ω_{p2}. This result only reflects the dependence of the single-particle excitation energy on magnetic flux (Fig. 2). The single-particle excitations also affect the strength of collective excitations. The weaker the Landau damping is, the higher the plasmon peak is. When ϕ is sufficiently large, a metallic carbon nanotube can exhibit one interband and intraband magnetoplasmon (the second magnetoplasmon at $\phi=0.02\phi_0$) or one interband magnetoplasmon and one intraband magnetoplasmon (the third magnetoplasmon at $\phi=0.025\phi_0$). The strength of the former is very strong because the intraband excitations are thoroughly combined with the interband excitations [Fig. 2(c)]. The intraband magnetoplasmon is heavily damped by the interband single-particle excitations of the $J=12$ energy band, so its strength is weak. Experimental measurements on it may be difficult. In short, the first, second, and third magnetoplasmons are, respectively, affected by the single-particle excitations of the energy bands of $J=24$, $J=24$, 12, and $J=12$. The resonant inelastic light-scattering measurements can be utilized to examine the collective and single-particle excitations.[40–42]

The direction of the magnetic field has an effect on the number of plasmon modes, plasmon frequency, and strength of plasmon, as shown in Fig. 3(b) at $\phi=0.01\phi_0$ and various α's. When α changes from 0° to 90°, the two interband magnetoplasmons are gradually getting into one interband mag-

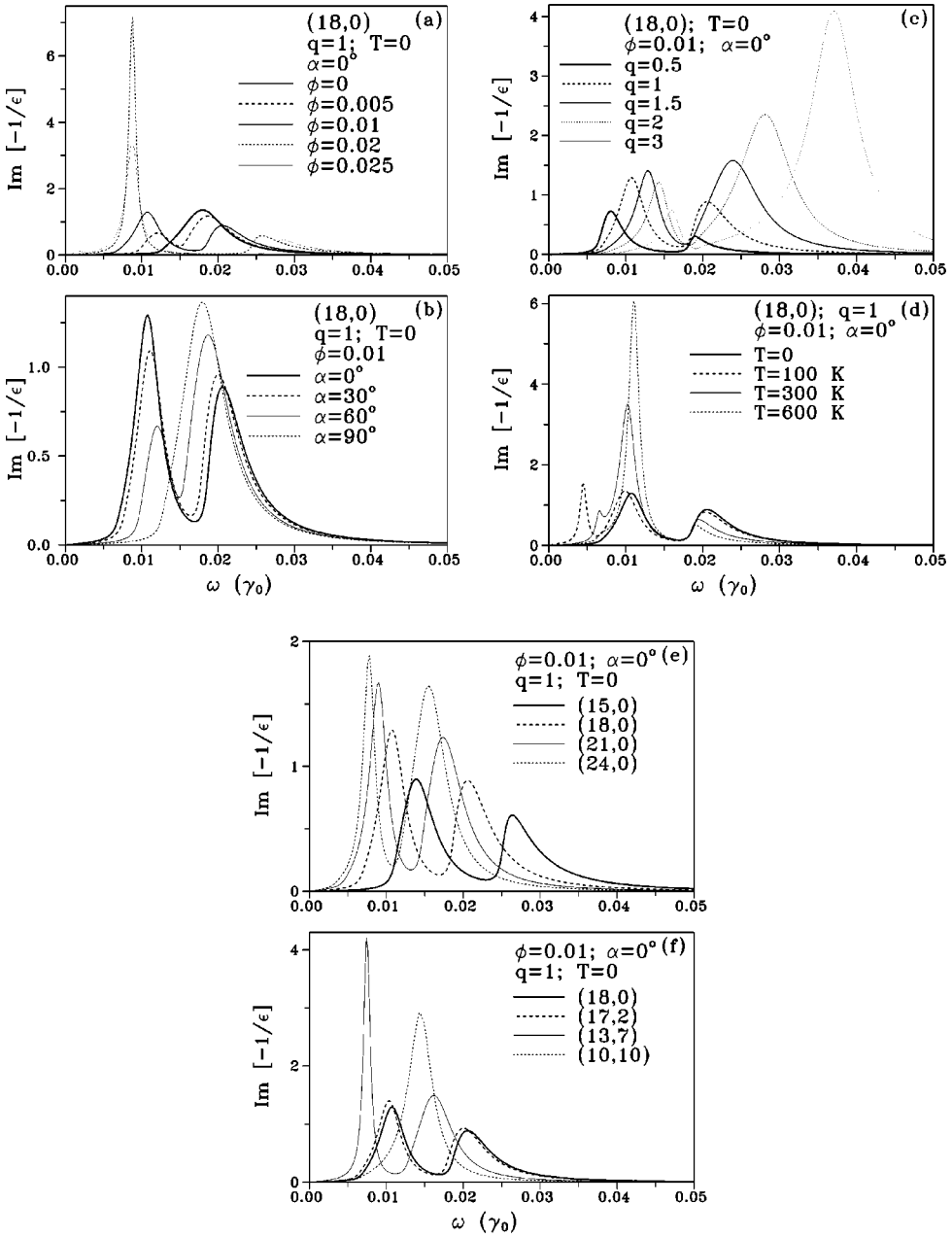

FIG. 3. Loss function of the (18, 0) zigzag nanotube calculated at various (a) ϕ's, (b) α's, (c) q's, (d) T's, (e) r's, and (f) θ's.

netoplasmon. For the second magnetoplasmon, the frequency becomes high, but the strength gets weak. The single-particle excitations from the $J=24$ energy bands make the strength of plasmon weaken. The first magnetoplasmon exhibits the opposite behavior. The main reason for the above-mentioned results is that the splitting of the $J=12$ and $J=24$ energy bands is gradually vanishing.

The loss function is apparently altered by the transformed momentum [Fig. 3(c)]. The single-particle excitation energies increase with q and so do the plasmon frequencies. The plasmon peaks become more prominent as q grows from zero. And then they will decay in the further increase of q. When q is too small or large, the plasmons are almost replaced by the single-particle excitations. The magnetoplasmons hardly survive below (q_{c1}) or beyond (q_{c2}) the critical momentum [Figs. 4(a) and 4(b)].

The temperature can induce the intraband excitations in a semiconducting carbon nanotube. Electrons will occupy the conduction bands at $T\neq 0$, $\phi=0.01\phi_0$, and $\alpha=0°$ [Fig. 1(b)]. Holes also exist in the valence bands. These two kinds of free carriers produce the intraband magnetoplasmon, as shown in Fig. 3(c). They even affect the first and second magnetoplasmons by means of reducing the interband excitation channels. The temperature needs to be sufficiently high to observe the prominent peak of the intraband magnetoplasmon. On the other hand, the intraband magnetoplasmon got mixed up with the second magnetoplasmon at high temperature ($T\geqslant 600$ K). The strength of the latter becomes very strong.

The nanotube geometry determines the low-energy bands and thus the magnetoplasmons. Figure 3(e) presents the loss

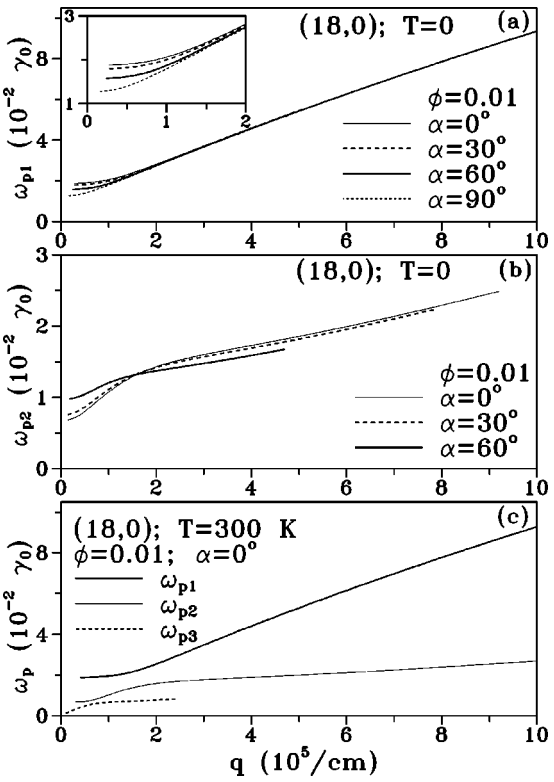

FIG. 4. Momentum-dependent plasmon frequency of the (18, 0) zigzag nanotube calculated at $\phi=0.01$, (a) $T=0$ and various α's for the first magnetoplasmon, (b) $T=0$ and various α's for the second magnetoplasmon, and (c) $T=300$ K and $\alpha=0°$ for three magnetoplasmons. The inset in (a) shows the details of ω_{p2} at small q.

functions for zigzag nanotubes with different radii. These nanotubes are semiconducting at $\phi=0.01\phi_0$ and $\alpha=0°$. Both the energy gap and curvature of energy bands decrease on increasing radius. The single-particle excitation energy and plasmon frequency behave so. The bare Coulomb interaction [Eq. (1)] and the single-particle excitations are also reduced. Their reductions lead to an enhancement of the strength of the plasmon. It is relatively easy to measure the low-frequency plasmons in large carbon nanotubes. The dependence of loss functions on the chiral angle is significant, e.g., those shown in Fig. 3(f) for various carbon nanotubes. All narrow-gap nonarmchair carbon nanotubes own two interband magnetoplasmons. However, a (m,m) armchair carbon nanotube exhibits one interband magnetoplasmon. That it only has low-energy bands of $J=m$ is the main reason. There is no simple relation between the chiral angle and the magnetic band structure (energy gap and curvature of energy bands). The plasmon frequency and the strength of plasmon are determined by the detailed magnetic band structures. They do not vary with the chiral angle monotonously.

The dispersion relations of magnetoplasmon frequency with momentum are important in understanding their characteristics. They are, respectively, shown in Figs. 4(a) and 4(b) for the first and second magnetoplasmons at $\phi=0.01\phi_0$ and various α's. The strong momentum dependence directly responds to the feature of the low-energy bands, the strong wave-vector dependence. This result means that the $L=0$ magnetoplasmon is the quantum of the collective electron oscillations propagating along the nanotube axis with a continuous wavelength $2\pi/q$. The plasmon frequencies approach finite values at small q; hence, the interband magnetoplasmons are optical plasmons. Also notice that the interband magnetoplasmons hardly survive at $q\rightarrow 0$. There are certain important differences between the first and second magnetoplasmons in the q- and α-dependent plasmon frequencies. The former exhibits a stronger q dependence, a larger critical momentum q_{c2}, and a simple relation between the plasmon frequency and α. The second magnetoplasmon is absent at $\alpha=90°$. Furthermore, it is relatively easily observed at small α.

Temperature somewhat affects the frequencies of the interband magnetoplasmons, as shown in Fig. 4(c). The intraband magnetoplasmon purely due to temperature owns the vanishing frequency at $q\rightarrow 0$. This plasmon should belong to an acoustic plasmon. It is in great contrast to the optical plasmons, the interband magnetoplasmons. At $T=300$ K, the intraband magnetoplasmon exists below the critical momentum $q\leqslant 2.4$. It is mixed up with or replaced by the second interband magnetoplasmon at larger momenta. The latter can exhibit a very prominent plasmon peak. The predicted momentum-dependent plasmon frequency can be verified by the resonant Ramman spectroscopy.[40–42]

In this work we have calculated for the narrow-gap or metallic carbon nanotubes the longitudinal dielectric function, which is useful in studying magnetic single-particle and collective excitations. The low-frequency single-particle and collective excitations, respectively, reveal themselves as the prominent peaks in the dielectric function and the loss function. They are significantly affected by the magnitude and direction of the magnetic field, transferred momentum, temperature, nanotube geometry, and Zeeman splitting. Resonant inelastic light scattering[40–42] can be used to test the calculated results such as the momentum-dependent plasmon frequency and single-particle excitation energy.

A narrow-gap nonarmchair carbon nanotube exhibits two interband magnetoplasmons, while a metallic nonarmchair carbon nanotube exhibits one interband magnetoplasmon and one interband and intraband magnetoplasmon or two interband magnetoplasmons and one intraband magnetoplasmon. An armchair carbon nanotube only exhibits one interband magnetoplasmon. The Zeeman splitting induces the overlap of the valence and conduction bands and thus the intraband magnetoplasmon or the intraband and interband magnetoplasmon. The differences among these magnetoplasmons are relatively obvious, when the magnetic field is oriented closer to the nanotube axis. The plasmon frequency (the strength of plasmon) increases (declines) as the nanotube radius decreases. A simple relation between the characteristics of plasmon and chiral angle is absent. The transferred momentum dominates the plasmon frequency and existence of plasmons. The temperature can cause an intraband magnetoplasmon or make an interband magnetoplasmon change into an intraband and interband magnetoplasmon.

This work was supported in part by the National Science Council of Taiwan, the Republic of China, under Grant Nos. NSC 91-2112-M-006-028 and NSC 91-2112-M-145-001.

[1] S. Iijima, Nature (London) **354**, 56 (1991).
[2] For the details of geometric structures see R. Saito, M. Fujita, G. Dresselhaus, and M. S. Dresselhaus, Appl. Phys. Lett. **60**, 2204 (1992); Phys. Rev. B **46**, 1804 (1992).
[3] J. W. Mintwire, B. I. Dunlap, and C. T. White, Phys. Rev. Lett. **68**, 631 (1992).
[4] J. W. Mintwire and C. T. White, Phys. Rev. Lett. **81**, 2506 (1998).
[5] C. T. White and T. N. Todorov, Nature (London) **393**, 240 (1998).
[6] J.-C. Charlier and Ph. Lambin, Phys. Rev. B **57**, 15037 (1998).
[7] N. Hamada, S. I. Sawada, and A. Oshiyama, Phys. Rev. Lett. **68**, 1579 (1992).
[8] C. L. Kane and E. J. Mele, Phys. Rev. Lett. **78**, 1932 (1997).
[9] For the details of curvature effects see F. L. Shyu and M. F. Lin, J. Phys. Soc. Jpn. **71**, 1820 (2002).
[10] H. Ajiki and T. Ando, J. Phys. Soc. Jpn. **62**, 1255 (1993).
[11] H. Ajiki and T. Ando, J. Phys. Soc. Jpn. **62**, 2470 (1993).
[12] H. Ajiki and T. Ando, J. Phys. Soc. Jpn. **64**, 4382 (1995).
[13] H. Ajiki and T. Ando, J. Phys. Soc. Jpn. **65**, 505 (1996).
[14] R. Saito, G. Dresselhaus, and M. S. Dresselhaus, Phys. Rev. B **50**, 14698 (1994); **53**, 10408(E) (1996).
[15] S. Roche, G. Dresselhaus, M. S. Dresselhaus, and R. Saito, Phys. Rev. B **62**, 16092 (2000).
[16] J. P. Lu, Phys. Rev. Lett. **74**, 1123 (1995).
[17] F. L. Shyu, C. P. Chang, R. B. Chen, and M. F. Lin, J. Phys. Soc. Jpn. (to be published).
[18] F. L. Shyu, C. P. Chang, R. B. Chen, C. W. Chiu, and M. F. Lin, Phys. Rev. B (to be published).
[19] M. F. Lin and K. W.-K. Shung, Phys. Rev. B **47**, 6617 (1993); **48**, 5567 (1993).
[20] O. Sato *et al.*, Phys. Rev. B **48**, 1947 (1993).
[21] P. J. Lin-Chung and A. K. Rajagopal, Phys. Rev. B **49**, 8454 (1994).
[22] P. Longe and S. M. Bose, Phys. Rev. B **48**, 18239 (1993).
[23] C. Yannouleas *et al.*, Phys. Rev. B **50**, 7977 (1994); **53**, 10 225 (1996).
[24] M. F. Lin, D. S. Chuu, C. S. Huang, Y. K. Lin, and K. W.-K. Shung, Phys. Rev. B **53**, 15493 (1996).
[25] B. Vasvari, Phys. Rev. B **55**, 7993 (1997).
[26] M. F. Lin, D. S. Chuu, and K. W.-K. Shung, Phys. Rev. B **56**, 1430 (1997).
[27] M. F. Lin and D. S. Chuu, J. Pulp Pap. Sci. **66**, 757 (1997).
[28] M. F. Lin and D. S. Chuu, Phys. Rev. B **57**, 10183 (1998).
[29] M. F. Lin and F. L. Shyu, Phys. Rev. B **60**, 14434 (1999).
[30] T. Stockli, J. M. Pitarke, A. Chatelain, Z. L. Wang, and P. Stadelmann, Phys. Rev. B **64**, 115424 (2001).
[31] G. Gumbs and G. R. Aizin, Phys. Rev. B **65**, 195407 (2002).
[32] R. Kuzuo, M. Tarauchi, and M. Tanaka, Jpn. J. Appl. Phys., Part 2 **31**, L1484 (1992).
[33] L. A. Bursill, P. A. Stadelmann, J. L. Peng, and S. Prawer, Phys. Rev. B **49**, 2882 (1994).
[34] T. Pichler, M. Knupfer, M. S. Golden, J. Fink, A. Rinzler, and R. E. Smalley, Phys. Rev. Lett. **80**, 4729 (1998).
[35] M. Kociak, L. Henrard, O. Stephan, K. Suenaga, and C. Colliex, Phys. Rev. B **61**, 13936 (2000).
[36] B. W. Reed and M. Sarikaya, Phys. Rev. B **64**, 195404 (2001).
[37] Q. P. Li and S. Das Sarma, Phys. Rev. B **44**, 6277 (1991).
[38] L. Wendler and V. G. Grigoryan, Phys. Rev. B **54**, 8652 (1996).
[39] M. Bayer, Ch. Schlier, Ch. Greus, A. Forchel, S. Benner, and H. Haug, Phys. Rev. B **55**, 13180 (1997), and references therein.
[40] A. R. Goni, A. Pinczuk, J. S. Weiner, J. M. Calleja, B. S. Dennis, L. N. Pfeiffer, and K. W. West, Phys. Rev. Lett. **67**, 3298 (1991).
[41] R. Strenz, U. Bockelmann, F. Hirler, G. Abstreiter, G. Bohm, and G. Weimann, Phys. Rev. Lett. **73**, 3022 (1994).
[42] E. Ulrichs, G. Biese, C. Steinebach, C. Schuller, D. Heitmann, and K. Eberl, Phys. Rev. B **56**, 12760 (1997), and references therein.